LRP 761/03 May 2003

Effects of localised electron heating and current drive on the sawtooth period

C. Angioni, T.P. Goodman, M.A. Henderson,
O. Sauter

accepted for publication in
Nucl. Fusion

ISSN 0458-5895

Effects of localised electron heating and current drive on the sawtooth period

C. Angioni[1], T.P. Goodman, M.A. Henderson, O. Sauter
Centre de Recherches en Physique des Plasmas,
Association EURATOM - Confédération Suisse,
Ecole Polytechnique Fédérale de Lausanne,
1015 Lausanne, Switzerland
[1]Present address: Max-Planck Institut für Plasmaphysik,
IPP-EURATOM Association, D-85748 Garching bei München, Germany

Abstract. Localised electron heating and current drive, like those produced by electron cyclotron heating (ECH) systems, are powerful tools for controlling the sawtooth period. They allow the direct modification of the plasma parameters which determine the sawtooth stability. In this paper we report a set of new experimental results obtained in the Tokamak à Configuration Variable (TCV) and a set of related simulations obtained applying a sawtooth period model in a transport code. The TCV device, equipped with a very flexible and powerful ECH system, is specifically suited for this kind of studies. In previous works, the experimental behaviour observed in TCV and JET was found consistent with a sawtooth period model first proposed to predict the sawtooth period in burning plasmas. In the present work, new experimental results have motivated a set of simulations which allow the identification of the effects of localised heating and current drive separately. In particular, two heating locations exist at opposite sides of the $q = 1$ surface which allow most efficiently sawtooth stabilisation and destabilisation. Moreover, the modelling shows that counter– and co– current drive alone, without the presence of heating, have opposite effects on the sawtooth period at symmetrical locations as compared with the position of the $q = 1$ surface. The main features of the experimental behaviour can be explained as due to the modification of the local plasma parameters involved in the linear resistive stability threshold of the internal kink, in particular the dynamics of the magnetic shear at the $q = 1$ surface. However it is shown that the most effective locations to modify the sawtooth period are not exactly at $q = 1$.

PACS numbers : 52.35.Py, 52.50.Sw, 52.55.Fa

1. Introduction

Sawtooth activity plays an important role in determining both plasma performance and plasma profiles. In particular, sawtooth stabilisation produces centrally peaked temperature profiles and therefore it can be regarded as favourable for increasing the fusion yield. On the other hand it has been shown that long sawtooth periods can have undesirable consequences, such as the creation of seed magnetic islands capable of triggering pressure limiting neoclassical tearing modes (NTMs) [1]. Moreover, sawtooth activity facilitates the removal of impurities from the plasma core, which is a particularly advantageous effect in the presence of helium ashes in a burning plasma. Therefore it is reasonable to envisage that the plasma performance and the fusion yield are a non-monotonic function of the sawtooth period, and that a specific length of the sawtooth period has to be identified in order to maximise both. For this reason it is of interest for the design of future nuclear fusion experimental devices to explore the efficiency of operational tools capable of modifying and controlling the sawtooth period. Among the various possible additional plasma heating systems, electron cyclotron heating (ECH) turns out to be particularly promising for this purpose. ECH makes it possible to attain very high values of heating power density, which affect locally various plasma parameters relevant to the sawtooth stability. Moreover, ECH allows current drive (ECCD), which has a direct effect in the modification of the plasma current profile.

From the first appearance of ECH, it has been observed in several tokamaks that the sawtooth period is particularly sensitive to ECH, and especially when the ECH deposition is close to the inversion radius [2–7]. However there remains a sort of uncertainty on the exact determination of the detailed effects of localised heating at different plasma locations, and in particular whether stabilisation is obtained when heating exactly at the $q = 1$ surface or just outside. Moreover, the effects of ECCD in those previous works were poorly explored. Later, other works have focused on the effects of ECCD as well, in particular in T-10 [8], FTU [9], JT-60U [10], WT-3 [11] and RTP [12]. Depending on the position of the absorbing layer with respect to the location of the $q = 1$ surface, different effects of co- and counter-CD have been observed.

Theoretical models have been proposed from the first experimental observations on sawtooth oscillations, in order to explain the experimental results. These first theoretical attempts were focused mainly in the explanation of fast particle stabilisation. Early attempts have been also dedicated to the theoretical description of ECH effects on sawteeth, in particular observed in TFR [13]. However at that time the theoretical understanding of the $m = 1$ magnetohydrodynamical (MHD) instabilities was still rather limited. The development of theoretical models describing the physics of the internal kink in various regimes have allowed, more recently, the introduction of more and more comprehensive models describing the thresholds of the sawtooth instability (e.g. [14, 15]). Moreover, the comparison between theory and experiment was rendered particularly difficult, and in most cases inconclusive, by the impossibility of measuring precisely the local plasma parameters at the $q = 1$ surface.

The Tokamak à Configuration Variable (TCV) [16] is a unique facility to explore the influence of EC on sawteeth [17–21]. In particular, several experiments have been performed during last years highlighting strong effects of ECH and CD on the sawtooth period [18, 20]. A relatively recent sawtooth period model [15] first proposed to predict the sawtooth period in the International Thermonuclear Experimental Reactor (ITER) [22] has been found consistent with several different aspects of the experimentally observed sawtooth period behaviour in TCV [19, 23–26]. This model provides triggering conditions for the sawtooth crash based on the linear stability thresholds of the internal kink in different ideal or resistive instability regimes. It also provides

prescriptions for the post-crash relaxed profiles, by means of a model for complete or partial reconnection based on the Kadomtsev model [27]. Our approach in the application of the model is to overcome the problem of the determination of the plasma parameters at the $q = 1$ surface, involved in the sawtooth period model, by applying the sawtooth model in a transport code. The self-consistent plasma parameters are therefore directly provided by the transport simulation.

This approach has been already used in simulations performed with the transport code PRETOR [28] and has been found successful and reliable in recovering the experimental behaviour of both Ohmic [23] and ECH [24, 25] discharges in TCV. Obviously it is necessary to have a fully consistent transport simulation, solving the diffusion equation for the poloidal magnetic field and coupling the transport code with an accurate equilibrium solver.

In the present paper, we identify the separate effects of localised heating and CD along the full plasma minor radius, with the purpose of providing a detailed understanding of the main physical effects at play such that simple recipes can be drawn on how to control the sawtooth period in a tokamak experiment.

We have performed a set of experiments in TCV using the specific feature of its ECH system, namely the steerable launching mirrors, and therefore the possibility of sweeping the beams along the plasma minor radius during a single plasma discharge.

The experimental results have motivated a set of simulations in order to single out the effects of CD separately from the heating. This is not possible in the experiments, since current drive is always accompanied by electron heating. In addition, the application of the model provides a physical understanding of the experimental observations and identifies the plasma parameters which play the crucial role in affecting the sawtooth period.

As a first step we address the specific and important issue of the identification of heating locations in the plasma which most efficiently stabilise or destabilise sawteeth. Then we present specific simulations intended to single out the effects of CD alone, co and counter. CD effects turn out to be opposite and symmetric with respect to the location of the $q = 1$ surface. At a same location heating and CD can produce very different effects, which account for the complex behaviour observed in experiments in which both current drive and heating are present at the same time.

The remainder of the article is organised as follows. In Section 2 a short presentation of the sawtooth period model and of the simulation methodology is provided. In Section 3 the experimental set–up and in particular the ECH system available at TCV are briefly reviewed. In Section 4 we present in detail experimental results and simulations which allow the identification of the heating location which most efficiently stabilises sawteeth. Effects due to the modification of the heating power density as obtained from the model and compared with TCV results previously published are also discussed. The relevant physical parameters involved in the model and which imply the variation of the sawtooth period as a response of the different heating conditions are pointed out. In Section 5 we describe a set of new experimental results and we present a related simulation which allows the identification of the heating location which most efficiently destabilises sawteeth. Section 6 presents the simulations intended to single out the effects of CD alone, and discusses the sawtooth period behaviour obtained when CD and ECH are combined. Conclusions about the present work are then drawn in the last Section.

2. Model for the sawtooth period and simulation methodology

The sawtooth period is simulated by the transport code PRETOR [28], in which sawtooth crash triggering conditions have been implemented as determined by linear stability thresholds of the ideal and resistive internal kink and included in the sawtooth period model proposed by F. Porcelli et al. [15].

In the remainder of the paper we shall refer to the transport code, the included sawtooth period model, and the modelling set–up described in the present section, as PRETOR–ST.

The transport code computes at each time step the temperature profiles and self-consistently the current density profile, solving a diffusion equation for the poloidal magnetic field. The plasma conductivity is assumed neoclassical and computed with formulae of Ref. [29], which include effects of both collisionality and plasma shape. The heat conductivity is taken from the Rebut-Lallia-Watkins local transport model [30], which has been found particularly successful in simulating the electron temperature in TCV in many different heating conditions and plasma shapes [31]. A two dimensional equilibrium solver is coupled and updates at each time step in the simulation the flux surface configuration.

The density profile is taken as input from the experimental measurements and kept fixed during the simulation. This approximation is somewhat rough, since the experimental behaviour of the density shows that, in the presence of localised heating, sawtooth activity has strong effects on both temperature and density profiles [21]. Nevertheless our approximation becomes necessary since, unlike the electron temperature, the density behaviour is quite difficult to be correctly simulated by the transport code. Models for the particle diffusivity have not yet been demonstrated as successful in the simulation of the electron density in the presence of intense localised electron heating. Moreover, although the local pressure gradient at the $q = 1$ has a crucial role in the sawtooth crash triggers, we assume that during the sawtooth ramp the variation of the local density gradient is small as compared with the variation of the temperature gradient.

A sawtooth period model suited for implementation in a transport code provides triggering conditions which predict when a sawtooth crash occurs during the transport simulation. Moreover, it has to provide prescriptions to determine the relaxed (post–crash) current, density and pressure profiles. Since the crash time is much shorter than all the relevant transport time–scales, the crash is assumed instantaneous. Therefore, when a sawtooth crash is triggered, the profiles are directly modified to the relaxed state after–crash.

In the framework of the sawtooth period model proposed by F. Porcelli et al. [15], first we have to identify the relevant instability regime. As discussed in previous works [19, 23, 24, 31], in TCV experiments, for plasma shapes like those considered in the present work (elongation $\simeq 1.4$, triangularity $\simeq 0.4$), the relevant dynamics which governs the stability of the internal kink is determined by resistive MHD. The ideal internal kink is stable, and the stability threshold is a threshold against the $n = 1/m = 1$ magnetic reconnection. In this resistive regime the crash trigger is determined by the comparison between the highest mode growth rate and the diamagnetic and drift frequencies which provide the most important stabilising effect [15]. The following crash triggering condition is considered,

$$\max(\gamma_\rho, \gamma_\eta) > c_r \ (\omega_{*i}\, \omega_{*e})^{1/2} . \tag{1}$$

This condition was first proposed in Ref. [23] in order to consider plasmas with high ratio of electron to ion temperature like in TCV and has been found in satisfactory quantitative agreement with the experimental

behaviour in the detailed simulation of a set of discharges with different ECH conditions [24, 25]. In Eq. (1)

$$\gamma_\rho = \left(\frac{2\,(1+\tau)}{\pi}\right)^{2/7} \hat{\rho}_i^{4/7}\, S^{-1/7}\, s_1^{6/7}\, \tau_A^{-1}, \tag{2}$$

is the internal kink growth rate in the semi–collisional ion–kinetic regime [32], and

$$\gamma_\eta = s_1^{2/3}\, S^{-1/3}\, \tau_A^{-1}, \tag{3}$$

is the resistive growth rate. In previous formulae $\omega_{*\sigma} = (T_\sigma\,|dp_\sigma/dr|)/(eBp_\sigma r_1)$ is the diamagnetic frequency of particle species σ, $\tau = T_{e1}/T_{i1}$, $\hat{\rho}_i = \rho_i\,/\,r_1$, $\tau_A = \sqrt{3}R_0/c_A$, ρ_i being the ion Larmor radius, R_0 the major radius and $c_A = B/\sqrt{\mu_0 n_i m_i}$ the Alfvèn speed. Quantities evaluated at the $q = 1$ surface are indicated by the subscript "1", and so s_1 is the local magnetic shear at the $q = 1$ surface. $S = \tau_\eta/\tau_A$ is the magnetic Reynolds (Lundquist) number, with $\tau_\eta = \mu_0 r_1^2/\eta$ the resistive diffusion time (η being the resistivity). The coefficient c_r is a dimensionless numerical factor which depends on plasma parameters, in particular on plasma shape and collisionality. It can be regarded as the free parameter of the model. In all the simulations presented in this paper $c_r = 0.75$, a value which is not too far from the analytical limit $c_r \simeq 1$, obtained for collisionless plasmas with circular cross section.

As first noted in Ref. [33], since both growth rates γ_η and γ_ρ involve s_1, the triggering condition can be rewritten in the form

$$s_1 > s_{1\,\mathrm{crit}}, \tag{4}$$

where $s_{1\,\mathrm{crit}}$, the critical shear at $q = 1$, is given by different expressions depending on whether the internal kink becomes unstable in the resistive or ion–kinetic regime. The expressions for $s_{1\,\mathrm{crit}\,\rho,\eta}$, obtained inverting Eq. (2) and Eq. (3) respectively and implemented in the transport code PRETOR, are the followings

$$s_{1\,\mathrm{crit}\,\rho} = 1.12\, c_r^{7/6}\, \hat{\rho}_i^{1/2} \left(\frac{R_1}{\bar{r}_1}\right)^{7/6} \left(\frac{T_{i1}}{T_{e1}}\,\frac{\bar{r}_1^2}{L_{pi\,1}\,L_{pe\,1}}\right)^{7/12} S^{1/6}\, \beta_{i1}^{7/12}, \tag{5a}$$

$$s_{1\,\mathrm{crit}\,\eta} = 1.355\, c_r^{3/2}\, \hat{\rho}_i^{3/2} \left(\frac{R_1}{\bar{r}_1}\right)^{3/2} \left(\frac{T_{i1}}{T_{e1}}\,\frac{\bar{r}_1^2}{L_{pi\,1}\,L_{pe\,1}}\right)^{3/4} S^{1/2}\, \beta_{i1}^{3/4}, \tag{5b}$$

$$s_{1\,\mathrm{crit}} = \min\left(s_{1\,\mathrm{crit}\,\rho}, s_{1\,\mathrm{crit}\,\eta}\right). \tag{5c}$$

Note that in both cases there is a strong dependence on the local plasma parameters at $q = 1$.

Once the crash condition Eq. (4) is satisfied, the q profile is relaxed according to Kadomtsev complete reconnection model. The density and pressure profiles are flattened within the mixing radius while keeping the total number of particles and energy conserved. This model can appear too rough, in particular when simulating sawtooth periods with non–standard shapes, as those occurring with localised heating close to the inversion radius [21]. However it must be mentioned that no experimental evidence of systematic partial reconnections have been observed in TCV from two dimensional reconstructions of the plasma emissivity during sawtooth periods of different time shapes [21]. The adopted relaxation model can be regarded as a working hypothesis which is not invalidated by experimental observations and assumed for the sake of simplicity. As shown in detail in Section 4, the sawtooth periods are always much longer than the time the relevant plasma parameters take to leave the relaxed state. Therefore the uncertainties on the relaxation model become less relevant since the results turn out to be not closely dependent on the profile relaxation model adopted.

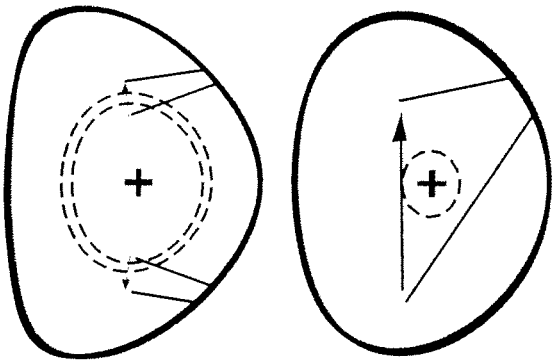

Figure 1. Poloidal cross sections of two TCV plasma boundaries, shot ♯21103 on the left, and shot ♯16053 on the right. Solid straight lines show the minimum and maximum poloidal injection angles used in the swept beam experiments, the arrows displaying the direction of the sweep. The dashed lines identify the $q = 1$ surfaces at the beginning and at the end of the sweep as obtained by the TCV equilibrium reconstruction code LIUQE.

3. Experimental set–up

TCV is a tokamak with major radius $R = 0.88$ m, minor radius $a = 0.25$ m, vacuum vessel elongation $k_V = 3$ and vacuum central magnetic field $B_0 \leq 1.54$ T. For the experiments considered in this work, TCV was operated with up to four 82.7 GHz, 500 kW gyrotrons, with a maximum of 2 s pulse length, for heating at the second electron cyclotron harmonic resonance using the extraordinary mode (X2). The X2 launchers are designed to direct the microwave beam at any radial location within the wide range of plasma shapes achievable on TCV. Each launcher has two degrees of freedom. The first provides steering of the beam in a fixed plane during a shot, realized by rotating the last mirror (48^o in 300 ms). The second degree of freedom allows that plane to be rotated about the axis of the launcher port between shots to introduce a toroidal injection angle (-180^o to +180^o). The first degree of freedom allows one to move the absorption location in the (minor) radial direction during a shot, the second allows one to produce controllable amounts of CD in both the co– and counter– directions. Local ECH flux surface averaged power densities in excess of 10 MW/m^3 have been obtained. The reference plasma on which sawtooth period experiments reported in this paper have been performed has the following parameters: limiter plasma, $I_p = 350$ kA, $B_t = 1.45$ T, $k = 1.4$, $\delta = 0.4$, line–averaged density $n_{el} = 1.6\ 10^{19}$ m^{-3}, $q_{edge} = 3$. Figure 1 shows two poloidal cross sections of TCV plasmas. The straight lines indicate the poloidal injection angle over which the beams are swept during the shot. The typical configuration adopted for the experiments presented in this paper is shown on the left of the figure, (shot ♯21103). The plasma cross section plotted on the right shows the configuration used in previous TCV experiments mentioned in Section 1, and further discussed in Section 3 [18]. Note the small window in the poloidal injection angle used in the recent experiments (Fig. 1, left). Nevertheless, variations of the sawtooth period of up to almost a factor 3 have been observed in these cases.

4. Stabilisation with localised heating

4.1. Brief overview of previous experimental results

The stabilising effect of ECH close to $q = 1$ was observed for the first time in the tokamak T–10 [2], to our knowledge, and the stabilising location was roughly identified as being outside the $q = 1$ surface. Experiments performed on other tokamaks have observed similar stabilising effects when heating at $q = 1$ or just outside

[6, 7, 39].

Experiments performed on TCV have shown the effect of heating on the sawtooth period and the sawtooth shape during magnetic field scans, vertical plasma displacements, and vertical beam displacements relative to a fixed plasma [17, 18, 20]. In particular, it has been shown that the sawtooth period and amplitude increase strongly when the power deposition crosses a given flux surface: there is a heating location in the plasma which inhibits the sawtooth instability. In these experiments it was observed that the heating location maximising the sawtooth period was close to the position of the inversion surface or the $q = 1$ surface, within experimental uncertainties. The authors were careful not to specify the precise location since on TCV there is no diagnostic measuring the current density profile so the position of the $q = 1$ surface is known only by equilibrium reconstruction using magnetic probes data. Furthermore, the spatial relation between the sawtooth inversion radius, determined for instance with the plasma soft X–ray (SXR) emissivity, and the $q = 1$ radius is not clear.

In the case of swept beam experiments [18, 20] the relatively high value of q_{edge} ($\simeq 4.5$) produced plasmas with small sawtooth inversion radii ($r_{inv}/a \sim 0.3$) which were determined with low resolution near the plasma centre, due to the relatively large pixel size of the X–ray tomography system (~3.5 cm). Determination of the absolute heating location with respect to the $q = 1$ surface in the plasma is also limited by errors in the reconstruction of the plasma equilibrium (particularly the vertical position) and subsequent ray tracing; although, reproducibility allows relative positioning to an accuracy of a few millimetres [18, 20].

Moreover, these swept beam experiments were performed with a full sweep from the bottom to the top of the plasma in 1 second (Fig. 1, right), a speed which does not allow to have many measurements of the electron density and temperature profiles by Thomson scattering in the time window during which the deposition location was close to the inversion surface. This increases the uncertainties when attempting to relate the deposition as computed by ray tracing, taking into account the experimental plasma profiles, with the rational surface as identified by equilibrium reconstruction consistent with the experimental pressure profile.

Detailed simulations of swept beam experiments [24, 25] with the code PRETOR have shown not only that the sawtooth model was able to capture the main features of the experimental behaviour, but also that the heating location maximising the sawtooth period is just outside the $q = 1$ surface.

4.2. New results: experiment and simulation determining the heating location for maximum stabilisation

In the present work recent shots at higher plasma current are analysed, allowing a more precise determination of the inversion radius. The higher plasma current implies a stronger Ohmic heating ($P_{OH} \simeq 0.47$ MW in the Ohmic phase, reduced to $P_{OH} \simeq 0.23$ MW in the ECH phase), and three launchers have been used with the deposition of the three beams superimposed on top of each other, with successful alignment, for a total of 1.35 MW of ECH power absorbed by the plasma. Moreover, the vertical beam sweep is slower than in previous experiments and is performed over a narrower plasma region, as it has been shown in Figure 1 (left). This makes the maximum location and its relation to the position of the $q = 1$ surface easier to determine. The narrow deposition window covered by the swept beams corresponds to injection angles within which the maximum sawtooth period has been observed in previous broader sweep experiments. It is interesting to note that the maximum sawtooth period (and the width of the sawtooth period peak in ρ_{dep}) is the same regardless of the sweep rates used to date. The slower sweep rates are helpful, however, to allow more accurate determination of the plasma parameters on TCV by providing more Thomson scattering measurements (each 50 ms) during

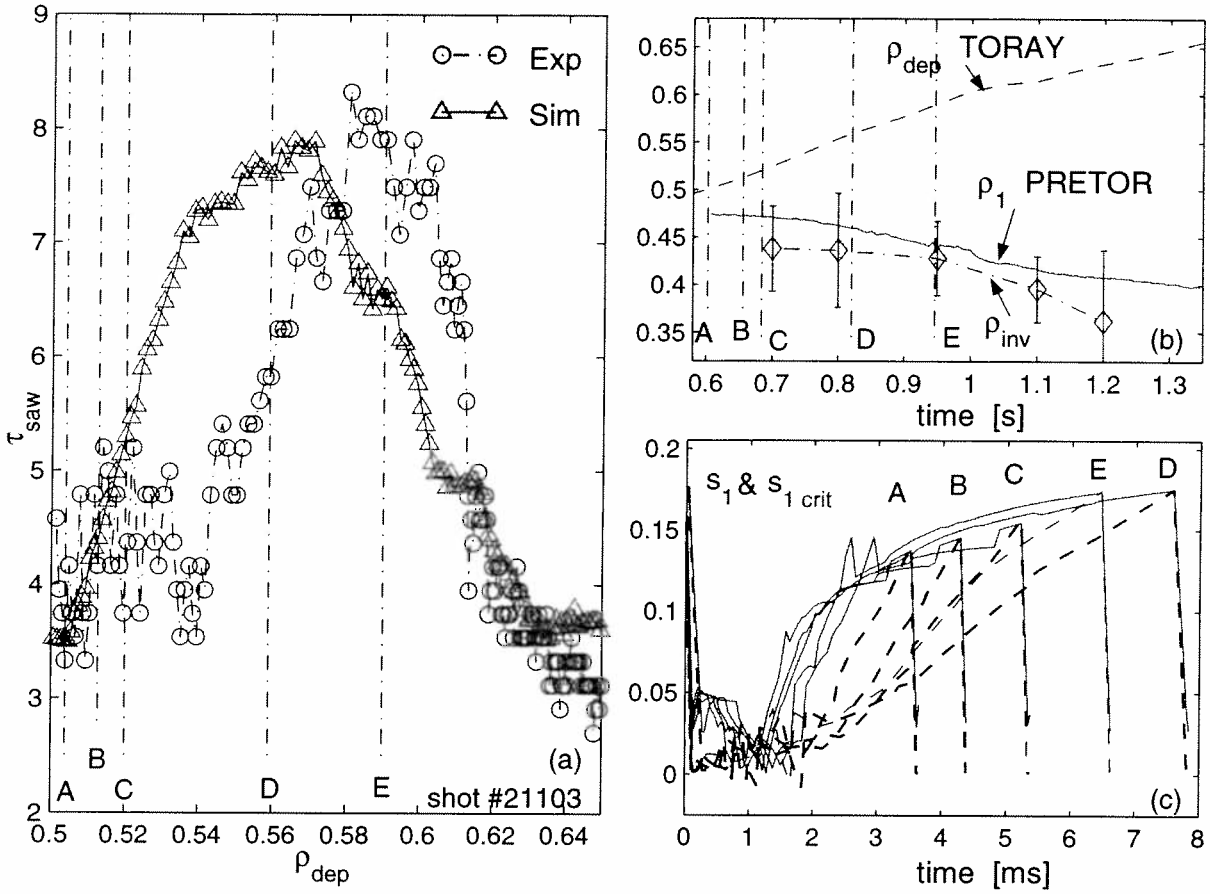

Figure 2. (a) Sawtooth period, measured (open circles) and simulated (open triangles), versus the ECH power deposition location for TCV shot ♯21103. Each marker point corresponds to a sawtooth crash. (b) Time trace of the simulated $q = 1$ radius before crash, compared with the measured sawtooth inversion radius and the power deposition location computed with TORAY-GA. (c) Time behaviour of the shear at $q = 1$ (dashed line) and the critical shear (solid line) for five sawtooth periods, as computed by PRETOR-ST during the simulation: the heating locations and time slices at the time of the sawtooth crashes are quoted in figures (a) and (b) by dash-dotted vertical lines and marked with letters 'A', 'B', 'C', 'D', 'E', respectively.

the scan of the peak. The results obtained in shot ♯21103 are shown in Figure 2. In Figure 2(a) circles show the evolution of the sawtooth period as a function of the power deposition. The power deposition location is identified with the weighted-average centre of the power density profile as computed with the ray-tracing code TORAY-GA [34-36]. The normalised radial coordinate is $\rho = \sqrt{V/V_{edge}}$, where V is the volume enclosed by the corresponding flux surface. With triangles we have plotted the corresponding sawtooth period as computed by a PRETOR-ST simulation performed using smoothed TORAY-GA power deposition profiles. From TORAY-GA the heating power density profile has a maximum ranging from 8 MW/m^3 at $\rho_{dep} \simeq 0.5$ to 6 MW/m^3 at $\rho_{dep} \simeq 0.65$, with a corresponding deposition width $\Delta\rho \simeq 0.08$. The simulation reproduces the variation of the sawtooth period, but exhibits a location maximising the sawtooth period ρ_{max} which is slightly shifted as compared to the experimental trace. Note however, that this shift is only of the order of $\Delta\rho \simeq 0.025$, that is 0.6 cm, which is below the errorbars on both the TORAY-GA deposition profile and the equilibrium reconstruction [37].

In Figure 2(b) the weighted–average centre of the TORAY–GA power density profile ρ_{dep} is plotted versus time. In the same figure we have plotted the time evolution of the $q = 1$ radius before crash as computed by PRETOR–ST during the simulation of the shot. We have also plotted the experimental inversion radius, determined from two dimensional reconstructions of soft X–ray (SXR) emissivity profiles [21]. Note first, that, as already mentioned, the experiment has been designed to sweep the power deposition in a narrow window covering the region in which the maximum sawtooth period was observed in previous sweep experiments covering a larger deposition window, and thereby also crossing the $q = 1$ surface. We observe that when the deposition is close to the PRETOR–ST $q = 1$ radius, or close to the measured sawtooth inversion radius, the sawtooth period is small, $\tau_{saw} \simeq 4$ ms, which is less than a factor of two longer than the Ohmic sawtooth period. By contrast, at the time of maximum sawtooth period, $\tau_{saw} \simeq 8$ ms, ρ_{max} is clearly outside the experimentally determined inversion radius, and the computed $q = 1$ surface, by $\Delta\rho \simeq 0.15$, that is more than 3 cm. This is larger than the errorbars in both the TORAY–GA power deposition profile and the self–consistent equilibrium reconstruction of PRETOR. This allows us to conclude that the heating location maximising the sawtooth period is outside the $q = 1$ surface. Second, the PRETOR–ST $q = 1$ radius is in good agreement with the measured sawtooth inversion radius. We acknowledge that the safety factor profile predicted by the transport code cannot be compared with experimental measurements at TCV, and this can be regarded as a limitation in the validation of the model, whose predictions strongly depend on the magnetic shear evolution. However, it must be mentioned that the same modelling set–up with the same transport code was applied in a previous work, to JET discharges, and a good agreement between the PRETOR–ST safety factor profile and the safety factor profile reconstructed with motional Stark effect measurements was found [38]. Third, both the PRETOR–ST $q = 1$ radius and the experimental inversion radius show the same decrease during the sweep as the power deposition location sweeps progressively further outside the $q = 1$ surface. This shows a general behaviour: the $q = 1$ surface moves inward when heating power is deposited outside this surface.

In Figure 2(c) we have plotted the time evolution of the relevant terms of Eq. (4), the shear s_1 and the critical shear $s_{1\,\mathrm{crit}}$ at the $q = 1$ surface, as computed by PRETOR–ST. We have chosen 5 sawtooth periods at five time slices during the simulation. These are identified in Figures 2(a) and 2(b) by dash–dotted vertical lines. (In Figure 2(c) the time quoted in x–axis has been rescaled to zero at the start of each sawtooth period for illustration purposes). The key role in determining the sawtooth period is played by the speed at which s_1 grows up during the sawtooth ramp. The shear s_1 is affected due to changes in the plasma conductivity caused by localised electron heating. The time evolution of the critical shear during the ramp is very similar in the five cases but, as ρ_{dep} approaches ρ_{max} the growth of the shear slows down ("A", "B", "C", "D"). When the power deposition moves outside, as shown by the sawtooth period marked with the letter "E", the growth of the shear is again more rapid. If the crash condition were simplified to $s_1 > s_{max}$, where s_{max} is a fixed value for the critical shear, independent of the plasma parameters, the corresponding sawtooth period variation obtained in the simulation would not be as large as the one observed experimentally, at least using the heating power density computed by TORAY–GA.

In the simulations, the time evolution of the parameters s_1 and $s_{1\,\mathrm{crit}}$ shows also that the sawtooth period is in any case much longer than the time taken by the plasma profiles to leave the relaxed post–crash state. This allows us to state that the relaxation model does not play a crucial role in determining the evolution of the sawtooth period. It should also be noted that due to the strong modification of the profiles after the crash, the numerical simulation takes 1-2 ms before the self–consistent profiles are well determined again (Fig. 2(c)). This

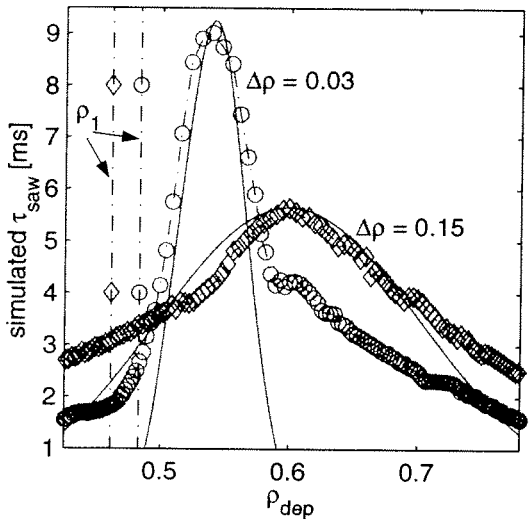

Figure 3. Simulated sawtooth period versus the heating power deposition location in the case of radial sweeps of Gaussian power deposition profiles: narrow profile ($\Delta\rho = 0.03$, plotted with diamonds) and broad profile ($\Delta\rho = 0.15$, plotted with circles). Each marker point corresponds to a sawtooth crash in the simulation. The solid lines show the power deposition profile at the time of the crash of the maximum sawtooth period, the plotted Gaussian profiles being centred at the corresponding values of ρ_{max} obtained in the simulations. Vertical dash-dotted lines mark the locations of the corresponding $q = 1$ radii.

is why PRETOR–ST cannot simulate sawtooth periods shorter than 2ms and with $s_{1\,\mathrm{crit}}$ smaller than 0.05-0.1 for usual TCV plasma parameters.

Although the plasma parameters of the model are computed at the $q = 1$ surface, it turns out that the heating location which most efficiently stabilises sawteeth is located outside $q = 1$. This heating location is determined by the power density applied, and therefore by the width of the power deposition profile. We emphasise also that simulations indicate that this heating location does not correspond to any specific physical surface. This is demonstrated by two representative simulations whose sawtooth period evolutions are plotted in Figure 3 and are discussed in the next subsection.

4.3. Effects of power density

We have simulated two sweeps in the radial direction of the heating power, considering two Gaussian power deposition profiles. The resulting sawtooth periods are plotted versus ρ_{dep}, the weighted-average centre of the deposition profile and therefore the centre of the Gaussian profile. We consider two representative deposition widths, $\Delta\rho = 0.03$ (circles) for very localised deposition, and $\Delta\rho = 0.15$ (diamonds) for broad deposition. The position of the $q = 1$ radius at the time of the maximum sawtooth period for the two cases are marked by dash–dotted vertical lines with circles and diamonds, respectively. These simulations are in good agreement with the experimental finding [40, 20] that the sawtooth period is a linear function of the power density: the maximum sawtooth period obtained in the simulation with localised heating is longer than that obtained in the simulation with a broad deposition profile (for the same total power). Furthermore, the simulations show that the curve of the sawtooth period versus ρ_{dep} reproduces the power deposition profile, plotted with solid lines in the two cases. The sawtooth period versus ρ_{dep} has a narrow peak in the case of localised deposition and a wide maximum in the case of broad deposition. This relationship between the sawtooth period trace and the

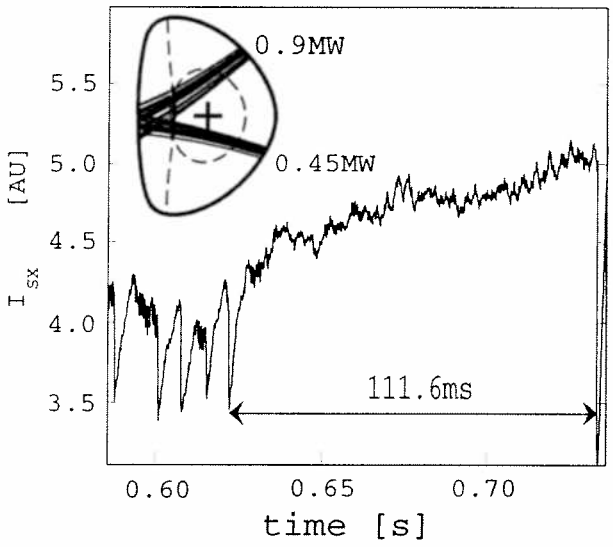

Figure 4. SXR signal and power deposition from TORAY-GA in the poloidal plane in the case of a shot with HFS deposition achieving sawtooth stabilisation for more than 110 ms. Three beams of 0.45 MW each are applied, achieving a power density of 15.6 MW/m^3 from TORAY-GA.

heating profile has been observed also experimentally in TCV, and is documented in Ref. [20]. This confirms the assumption that the response function of the sawtooth period versus the deposition location can be used to determine the power deposition profile [18]. The ability of the sawtooth period model to properly simulate these experimental observations incited us to place confidence in a prediction of the model which is more difficult to test experimentally.

We note that the distance between ρ_{max} and ρ_1 changes as a function of $\Delta\rho$, being narrower in the case of localised heating. From the simulations it results that $\rho_{max} - \rho_1$ is of the order of the power deposition width. Note that, in the specific case of narrow deposition profile in Figure 3, $\rho_{max} - \rho_1 \simeq 0.055$, that is ~ 1.5 cm. This distance is quite difficult to measure experimentally, given the uncertainties on the power deposition and the $q = 1$ position. However, in case of a wider deposition profile of the experimental result presented in Figure 2, the shift between ρ_{max} and ρ_{inv} has been experimentally detected. This simulation result makes the testable prediction that a wider beam profile should produce a maximum sawtooth period at a larger displacement from the inversion radius. Note that such an experiment must be performed with care to insure heating only (see Section 6).

The best position for stabilising sawteeth with ECH is therefore just outside the q=1 surface with a very localised power deposition in order to increase the power density at a given input power. The addition of co-CD helps as well, as will be shown below. The scenario which maximises the power density is when the deposition location is on the HFS at the equatorial plane (at $z = z_{axis}$). The HFS deposition was found to be more efficient for sawtooth stabilisation also in previous observations in WT-3 [7]. In this case, the beam deposition is tangent to the flux surface and even with a relatively large beam width, the deposition in $\Delta\rho$ is small (Figure 4). This was performed in TCV and is shown in Figure 4. In this case we obtained a very long sawtooth period, 110ms, of the order of the current redistribution time and about 50 confinement times. The effective deposition width is determined by the relativistic shift in this case which is small for ECH, and the absorbed power density exceeds 15 MW/m^3. Note that when co-CD is added, the current contributes to lengthen the sawtooth period

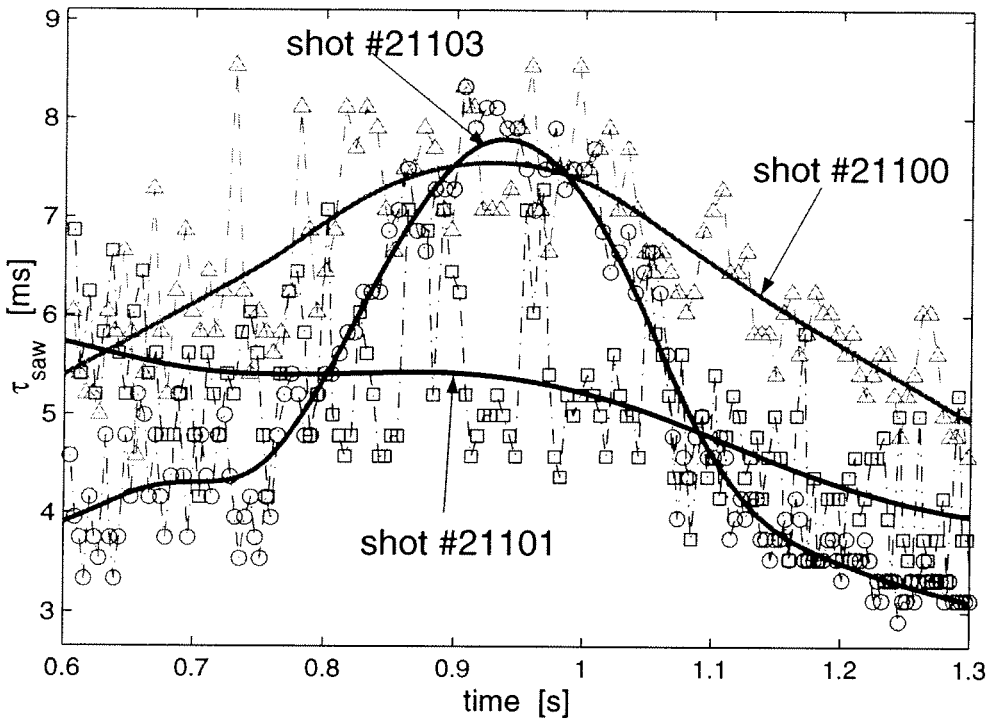

Figure 5. Sawtooth period time traces for three TCV discharges. Each marker point corresponds to a sawtooth crash. Solid lines provide best fits of the experimental points as visual guides. Shot ♯21103 (open circles) shows the sawtooth period response to a vertical sweep of three ECH beams, already presented and discussed in Figure 2. Shot ♯21101 (open squares) shows the sawtooth period response to a vertical sweep of three beams in the presence of a fourth beam aiming just inside the sawtooth inversion radius ($\rho_{dep} \simeq 0.33$). Shot s♯21100 (open triangles) shows the sawtooth period response to a vertical sweep of three beams in the presence of a fourth beam aiming at the plasma centre.

by modifying s_1 (Section 6), however the Doppler shift is larger and hence the deposition width increases. This is why the optimum experimental conditions depend on the launcher configurations and therefore can differ slightly between different plasma profiles and tokamaks.

5. Destabilisation with localised heating

A very interesting and unexpected feature has been observed in an experiment similar to the one discussed in the previous Section and presented in Figure 2 (shot ♯ 21103). A fourth beam aiming at a fixed location just inside the supposed position of the $q = 1$ surface ($\rho_{dep} \simeq 0.33$) has been added during a vertical sweep of three beams completely analogous to the one described in the previous Section. It has been observed that the maximum of the sawtooth period, usually obtained during a vertical sweep, was suppressed by the presence of the fourth beam (shot ♯ 21101 in Figure 5). Sawtooth periods of the order of 5 ms on average were obtained in place of periods of up to 8 ms, as in the experiment previously presented. It has also been observed that if the fourth beam is rather directed towards the plasma centre during the vertical sweep of the other three beams, the sawtooth period increases again during the sweep, reaching a maximum with values of the order of 7.5 ms (shot ♯ 21100 in Figure 5). This set of experiments suggests the presence of a heating location, just inside the $q = 1$ surface, which is the most effective to destabilise sawteeth.

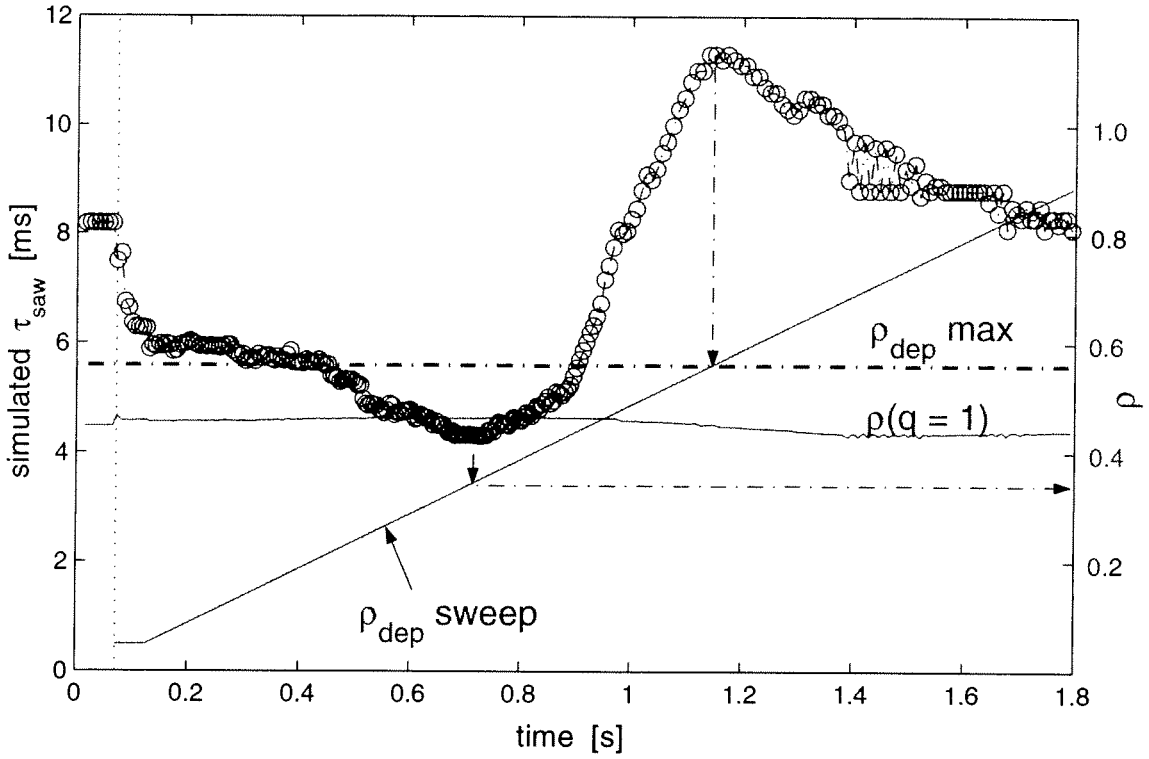

Figure 6. Simulated sawtooth period time trace in the case of a full radial sweep of localised 0.45 MW of electron heating, while stabilising sawteeth with 1.35 MW at the fixed location ρ_{max}. The simulation has the same plasma parameters as the experimental plasma of shot ♯21103. The values of the sawtooth period, circles, are quoted at the left, whereas values of the normalised minor radius ρ are quoted at the right. The time behaviour of the power deposition location ρ_{dep} of the sweeping beam is plotted with a solid line (the dotted vertical line at the left identifies the time slice at which the swept beam has been turned on). The horizontal dash–dotted line marks the location of ρ_{max}. The time trace of the $q = 1$ radius $\rho(q = 1)$ is plotted with a solid line.

5.1. Simulation of sawtooth destabilisation with localised heating

These experimental results have motivated a series of simulations in order to investigate the phenomenon. We have considered 1.35 MW, the equivalent of three gyrotron beams, fixed at the location maximising the sawtooth period, ρ_{max}, as determined with the simulation of shot ♯21103 and presented in Figure 2, that is at $\rho_{dep} = 0.56$. Therefore the sawtooth period at the beginning is about 8 ms, as expected from the maximum value obtained in the previous simulation. We apply a sweep of one beam of 0.45 MW starting from the plasma centre up to the edge. In the same way that an experiment of power sweep starting from ohmic conditions allows us to identify locations which provide sawtooth stabilisation, a sweep performed starting from heating conditions in which the sawtooth period is maximised allows us to better explore the existence of locations which most efficiently destabilise sawteeth.

The results are presented in Figure 6. The vertical dotted line at the left marks the beginning of the heating due to the fourth swept beam, which starts aiming at the plasma centre, $\rho_{dep} = 0.05$. The linear time evolution of the deposition location of this beam is plotted with a solid line. The maximising location, $\rho_{dep} = 0.56$, at which 1.35 MW are deposited permanently, is marked with a horizontal dash–dotted line. The time evolution of the radius of the $q = 1$ surface, computed self–consistently by PRETOR–ST in the simulation, is shown with

a solid line. The resulting sawtooth period is presented with circles.

Two heating locations are of particular relevance, and have been put in evidence by dash–dotted arrows in the Figure. One is the already known location ρ_{max}, at which the period is maximised. As expected, when the sweeping beam crosses this location, at which the fixed beams are aiming, the local power density is increased and so is the sawtooth period. An evident maximum is obtained.

The second relevant heating location is the one we were actually looking for. In agreement with the experimental results discussed at the beginning of the present Section, there is a heating region inside $q = 1$ which destabilises sawteeth, in this case between $\rho_{dep} = 0.25$ and 0.42. The location of the minimum in the present specific simulation turns out to be located at $\rho_{dep} = 0.35$, whereas the $q = 1$ radius is at $\rho_1 = 0.46$. This location is almost coincident to the location used in the experiment which allowed the suppression of the sawtooth period increase during the sweep of the other gyrotrons. Generally speaking, we can roughly state that symmetrically, on opposite sides of the q=1 radius, heating locally destabilises sawteeth when inside and stabilises sawteeth when outside.

The key parameter producing the sawtooth period variation in the simulation is still the magnetic shear at $q = 1$. The speed of its growth during the sawtooth ramp is strongly affected by the power deposition location, as already presented in detail in Figure 2(c). In particular, when heating inside $q = 1$, s_1 increases faster and reaches $s_{1\,\mathrm{crit}}$ earlier. Note also that the variation of the sawtooth period obtained in the present simulation is in good quantitative agreement with the actual periods observed in the experiments mentioned at the beginning of this Section.

The destabilising effect of localised heating inside $q = 1$ clarifies why the heating location providing maximum stabilisation predicted by simulations depends on the width of the power density profile, as presented in Figure 3. The broad heating profile provides maximum stabilisation when the centre of the deposition is sufficiently outside $q = 1$ to limit the fraction of the power which is absorbed inside $q = 1$, and which thereby has a destabilising effect (the modelling predicts roughly $\rho_{max} - \rho_1 \simeq 0.5\Delta\rho_{dep}$).

5.2. Experimental results with analogous set–up of the simulation

An experiment with analogous set–up of the simulation presented in Figure 6 has been recently performed to test the prediction of the sawtooth period model [41, 42]. In the experiment 0.9 MW of power, instead of 1.35 MW, was used at a fixed injection angle to simplify the overlap of the stabilising beams. In addition, a small co–ECCD component due to the poloidal field is also present. This should cause the maximum found in the simulation (heating only) to shift slightly inward and the minimum slightly outward (Section 6, Figure 8). The additional co–ECCD also increases the sawtooth period at the maximum relative to pure heating (Section 6, Figure 10). On TCV an additional beam was swept, similar to the simulation of Figure 6. The results are presented in Figure 7, as a function of time and ρ_{dep}. The EC power density contours are shown along with the $q = 1$ radius computed by the TCV equilibrium reconstruction code LIUQE [43]. The sawtooth period is then overlaid as a function of time. A general agreement with the simulation presented in Figure 6 is found. Starting from the stabilised sawtooth period (time < 0.8 s), the central beam is destabilising (time > 0.8 s), a small minor peak is found (time $\simeq 1.1$ s), and finally the beam crosses the location of the other 2 beams (time > 1.4 s) with a further increase in the sawtooth period. Following the minor peak at time $\simeq 1.1$ s, a minimum is observed in the period at time $\simeq 1.2$ s, whose value is not shorter than that found at the start of the sweep (the sawtooth amplitude, however, exhibits a minimum only at time $\simeq 1.2$ s). We must add that between 0.8 s

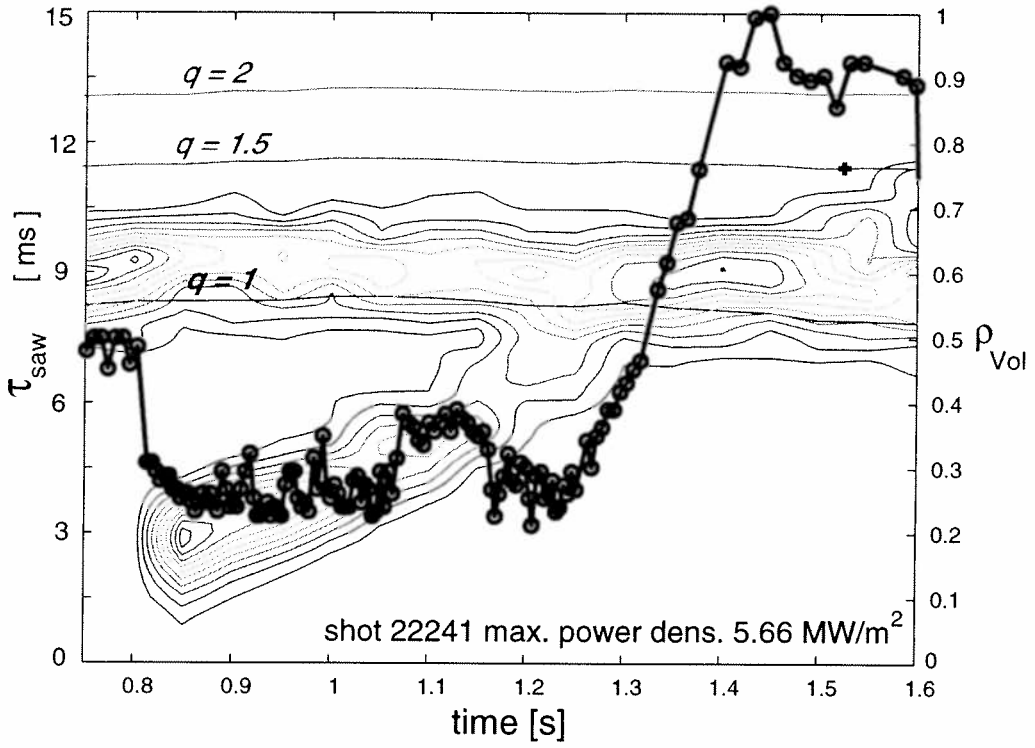

Figure 7. Experimental sawtooth period (open circles), LIUQE $q = 1$ radius (thick solid line), and TORAY–GA ECH power density contours: 0.9 MW ECH (slight co-ECCD) fixed for optimum stabilisation; 0.45 MW of swept ECH (slight co-ECCD). Localised heating is found to destabilise sawteeth inside $q = 1$.

and 1.05 s a 6 kHz mode activity is detected by the magnetic pickup coils, which is observed as a precursor to the sawtooth crash. At the minor peak (time $\simeq$ 1.1 s), this mode activity stops prior to causing a crash and the rise in the central SXR signal continues as before, up to the crash. This results in longer sawtooth periods. It is likely that short periods of sawteeth in the phase between 0.8 s and 1.05 s are due to the presence of the above mentioned mode activity. By contrast, during the minimum in sawtooth period at 1.2 s, no 6 kHz mode activity is detected, which indicates that this reduction of the sawtooth period must be ascribed to a different cause. This minimum is therefore likely to be due to local shear modifications induced by localised heating of the swept beam, in agreement with the simulation of Figure 6. In order to be able to completely follow the evolution of the sawtooth period in the presence of modes, and magnetic islands persisting during a non-negligible phase of the sawtooth ramp, a model capable of describing the effects of the interaction between the island and the ECH beam on the stabilisation of sawteeth should be developed. These are mainly 2D phenomena [21], which cannot be taken into account with our 1D modelling. In this sense, this experimental behaviour points out one of the limitations of the model, as also discussed in the conclusions (Section 7).

Nevertheless, at least for plasma conditions like those prevailing in this experiment, these effects are small, and in all the phase in which the swept beam is absorbed by the plasma inside the $q = 1$ surface, from time $\simeq$ 0.8 s to time $\simeq$ 1.3 s (from $\rho_{dep} \simeq 0.2$ to $\rho_{dep} \simeq 0.5$), the sawtooth period is in any case reduced as compared with the initial value. This is well in agreement with the prediction presented in Figure 6 and assesses also experimentally the destabilising effect of localised heating deposited inside the $q = 1$ surface.

6. Simulations of stabilisation and destabilisation with current drive

Since ECH can produce current drive, and since the sawtooth period is governed by variations in the dynamics of the magnetic shear at $q = 1$, ECH has another powerful capability to affect sawteeth, in addition to localised heating.

In TCV very strong effects of CD have been observed [18, 20]. In particular, very small amounts of CD (less than 5 kA in a 300 kA plasma) can be obtained with off–axis heating and with perpendicular toroidal injection, due to the presence of the poloidal magnetic field and therefore to the pitch of the magnetic field line. These small amounts of CD imply non–negligible variations of the sawtooth period. This effect has been already analysed with the present model in a specific simulation of two TCV discharges [24, 25]. It was found that counter–CD and co–CD when applied at ρ_{max} have opposite effects on the dynamics of the magnetic shear, provoking an acceleration or a slowing down respectively.

Since in the experiment CD is always accompanied by electron heating, it is only in the simulations that one can explore the effects of CD alone on sawteeth.

Here we present the results of simulations performed with the same set–up as presented in the previous Section. We keep 1.35 MW of heating power fixed at ρ_{max} and we compute the effect of a sweep of a small amount of localised CD, 3.5 kA, over the full minor radius. The same density profile has been taken in the simulations presented in this Section and in the previous Section. The results are presented in Figure 8. Both the case of co–CD (+3.5 kA) and counter–CD (–3.5 kA) are considered. These amounts of CD are of the order of 1% of the plasma current. At the plasma centre the local maximum driven current density (0.92 MA/m^2) is about 32% of the local current density, whereas at the $q = 1$ surface (0.11 MA/m^2) it is less than 4% of the local current density.

The sawtooth period evolution obtained in the simulation with co–CD is plotted with triangles pointing up, whereas the sawtooth period obtained with counter–CD is plotted with triangles pointing down. The stabilisation with counter–CD inside the $q = 1$ surface and co–ECCD outside, as well as the destabilisation with co–CD inside $q = 1$ and counter–CD outside, are consistent with experimental observations in JT–60U [10]. Moreover, the destabilising effect of co–CD and stabilising of counter–CD when applied inside the $q = 1$ surface is in agreement with experimental observations in RTP [12]. Finally, the stabilising effect of co–CD and destabilising of counter–CD when applied outside the $q = 1$ surface is in agreement with experimental observations in TCV [20], and was already found in previous simulations [24, 25]. These simulation results show also an overall qualitative agreement with recent results obtained on ASDEX Upgrade [44], in experiments involving neutral beam injection (NBI), ECH and ECCD. Note however that these experiments have been performed in the presence of a dominant amount of NBI heating. In this situation not only the ECH deposition location and CD, but also fast particle and plasma rotation effects, due to NBI, can affect the sawtooth period response. In particular, beam ions can provide a dominant contribution to the internal kink potential energy, and thereby change the relevant threshold triggering the sawtooth crash, as recently observed simulating the sawtooth period behaviour in JET discharges with beam ion stabilisation of sawteeth [38].

When considered alone, co– and counter–CD have opposite effects when deposited at symmetric locations about the $q = 1$ surface. This symmetry cannot be observed in the same way in the experiments, since heating, which is always present in reality, creates an additional asymmetry, as presented in Figure 6, which renders the experimental behaviour of the sawtooth period much more complex, especially in the case of counter–CD. Indeed

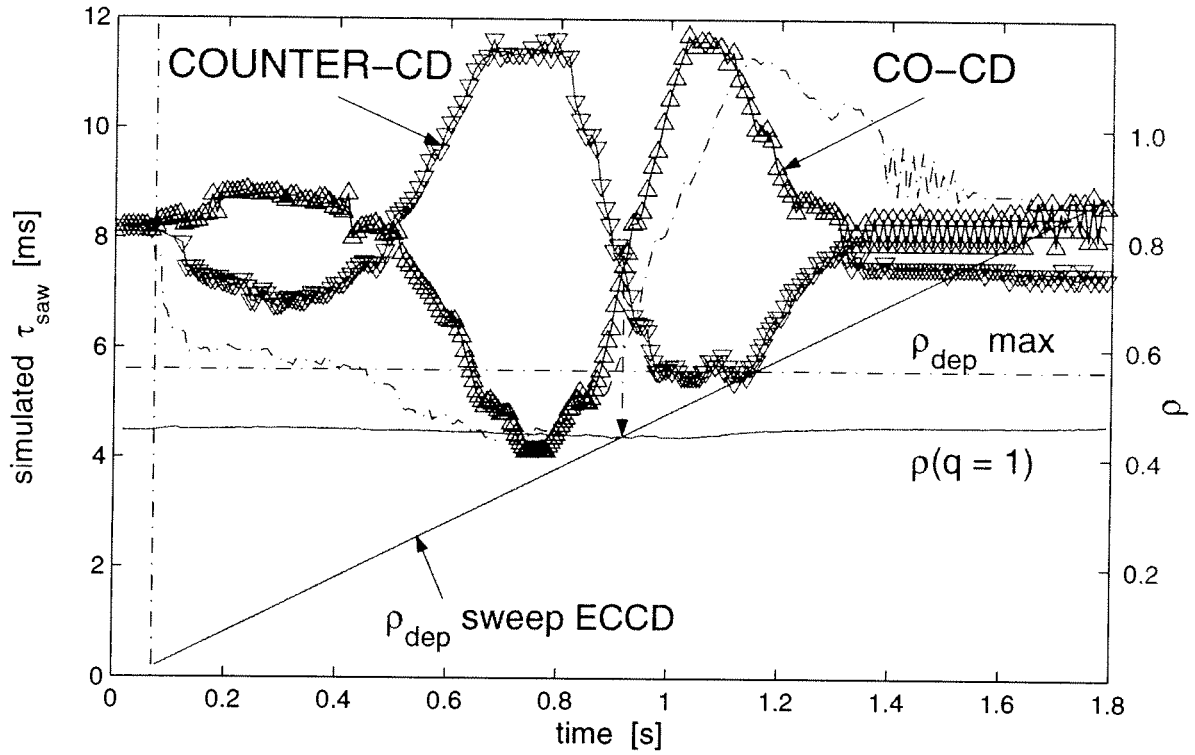

Figure 8. Simulated sawtooth period time traces in the case of full radial sweeps of a localised and small amount of current drive (3.5 kA), in the case of stabilised sawteeth with 1.35 MW at the heating location ρ_{max}. The simulated sawtooth period response to the sweep of co–CD is plotted with triangles pointing up, whereas the response to the sweep of counter–CD is plotted with triangles pointing down. The dash–dotted curve shows for comparison the sawtooth period behaviour in the case of a sweep of localised heating, already presented in Figure 6. The values of the sawtooth period are quoted on the y–axis at the left. Time traces of the normalised location ρ_{dep} of the sweeping CD, as well as of ρ_{max} and $\rho(q = 1)$ are plotted in the same way as in Figure 6, and quoted on the y–axis at the right.

co–CD effects on the sawtooth period are similar to those of localised heating, whereas counter–CD effects are opposite. The trace of the sawtooth period obtained in the simulation with a sweep of localised heating (already presented in Figure 6) has been added in Figure 8 with a dash–dotted line in order to provide a reference. It appears also that the most efficient location for CD to stabilise in the case of co–CD, and destabilise in the case of counter–CD, are slightly shifted closer to the $q = 1$ surface compared with heating alone. This implies that particularly in the presence of both counter–CD and localised heating, complex and multi-maximum time traces of the sawtooth period can be expected when the resonance approaches the $q = 1$ surface, since the sawtooth period results from opposite and competitive effects obtained in very localised plasma regions. This is shown by the simulations presented in the next subsection.

6.1. Simulations of combined effects of heating and current drive

In Figure 9 we have plotted the sawtooth period behaviour versus the deposition location ρ_{dep} of the swept beam for four different simulations. The dashed line shows the case of only heating, already presented in Figure 6, whereas the solid line represents the case of counter–CD alone, already presented in Figure 8. These curves have been plotted to provide reference behaviours in order to understand the results provided by the new simulations. The dash–dotted line with circles shows the sawtooth period behaviour when both heating and

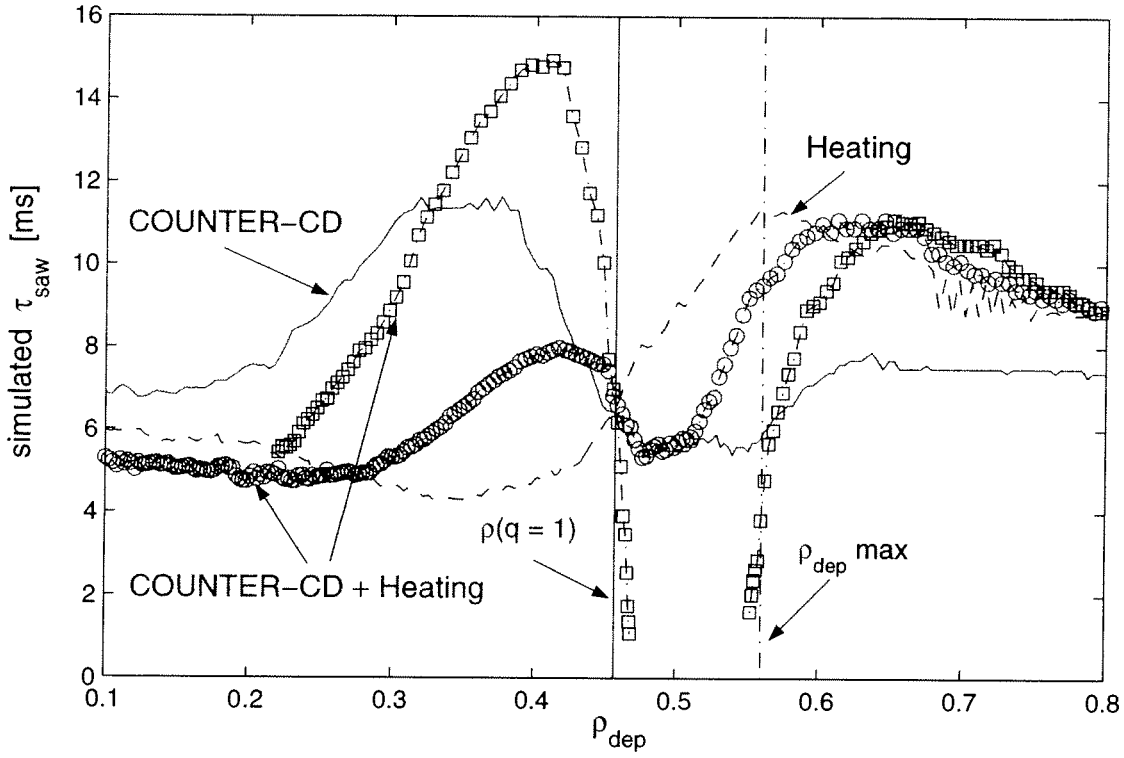

Figure 9. Simulation of the evolution of the sawtooth period versus the deposition location of a swept beam, while stabilising sawteeth with 1.35 MW ECH at $\rho = \rho_{max}$. The dashed line shows the sawtooth period evolution when the swept beam produces 0.45 MW of heating, the solid line shows the case when the swept beam produces -3.5 kA of counter–CD only. The dash–dotted line with open circles shows the evolution of the sawtooth period when the swept beam produces 0.45 MW of heating *and* drives -3.5 kA of counter–CD. The dash–dotted line with open squares shows the evolution of the sawtooth period when the swept beam produces 0.45 MW of heating *and* drives -10 kA of counter–CD.

counter–CD are applied at the same time, using the same amounts as in Figs. 5 and 6, that is 0.45 MW and -3.5 kA respectively. The dash–dotted line with squares shows a simulation in which the same amount of localised heating is accompanied by a larger amount of counter–CD, -10 kA. In this case the sweep has been started at $\rho_{dep} = 0.2$ since for central depositions the CD density is large enough to produce a reversed safety factor profile, which is outside the validity domain of the model for both the sawtooth period and the post–crash profile relaxation.

These simulations show that the sawtooth period results from a superposition of effects coming from both localised heating and counter–CD. When the deposition is inside the $q = 1$ surface, counter–CD and heating have opposite effects, stabilising the first and destabilising the second. Depending on the relative amounts of CD density and heating power density different effects can be obtained. The simulation shows that the effect due to CD prevails already at relatively low values of driven current. With a deposition outside the $q = 1$ surface, the shift between the location maximising the sawtooth period with heating alone (dashed curve) and the location minimising the sawtooth period with counter–CD alone (solid curve) imply a strong oscillation of the sawtooth period as a function of ρ_{dep} when both counter–CD and heating are simultaneously at play in the swept beam. A minimum is found just outside $q = 1$, due to CD effects, and a maximum is found outwards, due to localised heating effects.

This behaviour is similar to that recently observed in JET experiments with ion cyclotron resonance heating [45], involving small components of both co– and counter–CD at shifted locations as compared with the location of the electron collisional heating power deposition. The sawtooth period has been observed to oscillate producing a time trace with two maxima when the resonance approaches and crosses the inversion radius from outside to inside [45]. The complex sawtooth behaviour observed with ICRH and ICCD at JET can therefore be understood as due to the superposition of different and competitive effects, due to localised heating and CD, and is consistent with the separate effects as observed and identified in ECH experiments. This explains why PRETOR–ST was successful in simulating these effects [46].

When a larger amount of counter–CD is applied (dashed–dotted line with squares in Figure 9) the sawtooth period is completely destabilised just outside $q = 1$, providing sawtooth periods in the simulation which are below 1 ms. Therefore counter–CD outside the $q = 1$ surface allows the "suppression" of the sawtooth oscillation, although not obtained with a "stabilisation": sawteeth can be suppressed either as the sawtooth period goes to infinity (complete stabilisation), or as the sawtooth period goes to zero and is infinitely small (complete destabilisation). Counter–CD provides the second effect when applied just outside the $q = 1$ surface, while, when applied inside $q = 1$, it is strongly stabilising, prevailing over the destabilising effect of localised heating. It is important to remember that in all these simulations, 1.35 MW of heating power is constantly being deposited at ρ_{max}.

The relative effects of counter–CD stabilisation and heating destabilisation with a deposition just inside the $q = 1$ surface ($\rho_{dep} = 0.4$) have been explored by the simulation of a CD ramp–up, keeping fixed values of the heating powers: 1.35 MW have been deposited at $\rho_{dep} = 0.56$, whereas 0.45 MW have been deposited at $\rho_{dep} = 0.4$. At this location a ramp in the counter driven current has been simulated, from -3.5 to -23.0 kA of counter–CD. The simulated sawtooth period is found to increase linearly with increasing amount of CD, highlighting that CD is more efficient than heating in affecting the sawtooth period. The linear behaviour has been observed experimentally in TCV, although only for smaller amounts of CD [20]. No asymptotic saturation to a full stabilisation has been observed in the simulation: note however that the simulation results become questionable at high amounts of CD, when the shape of the safety factor profile starts to be strongly affected and the analytical expressions for the contributions to the internal kink energy functional [15] used in the model give only very approximated estimates. Furthermore the model is limited to amounts of CD which do not imply reverse safety factor profiles or safety factor profiles with more than one $q = 1$ surface.

Analogous simulations to those shown in Figure 9, but this time involving co–CD, are presented in Figure 10. Circles show the sawtooth period time trace obtained with the radial sweep of 0.45 MW of heating power and 3.5 kA of co–CD, whereas the simulation results plotted with squares have the same amount of power and 10 kA of co–CD. The destabilising effects of both co–CD and ECH when applied just inside the $q = 1$ surface lead rapidly to complete suppression of sawteeth, in the same way that it has been observed for counter–CD, but just outside $q = 1$. The co–CD effect on top of the ECH effect allows the most efficient stabilisation of the sawtooth oscillation, when applied just outside the $q = 1$ surface. This has been assessed with the simulation of a co–CD ramp at the maximum period location, analogous to that described for counter–CD.

The strong stabilisation induced by CD, both with counter–CD inside $q = 1$ and with co–CD outside, is obtained in the model since with increasing amounts of CD the s_1 and $s_{1\,\mathrm{crit}}$ time traces become more and more parallel, preventing the trigger condition from being reached. Note in this sense that CD affects the time evolution of both s_1 and $s_{1\,\mathrm{crit}}$. This is because the dynamics of the $q = 1$ surface expansion during the sawtooth

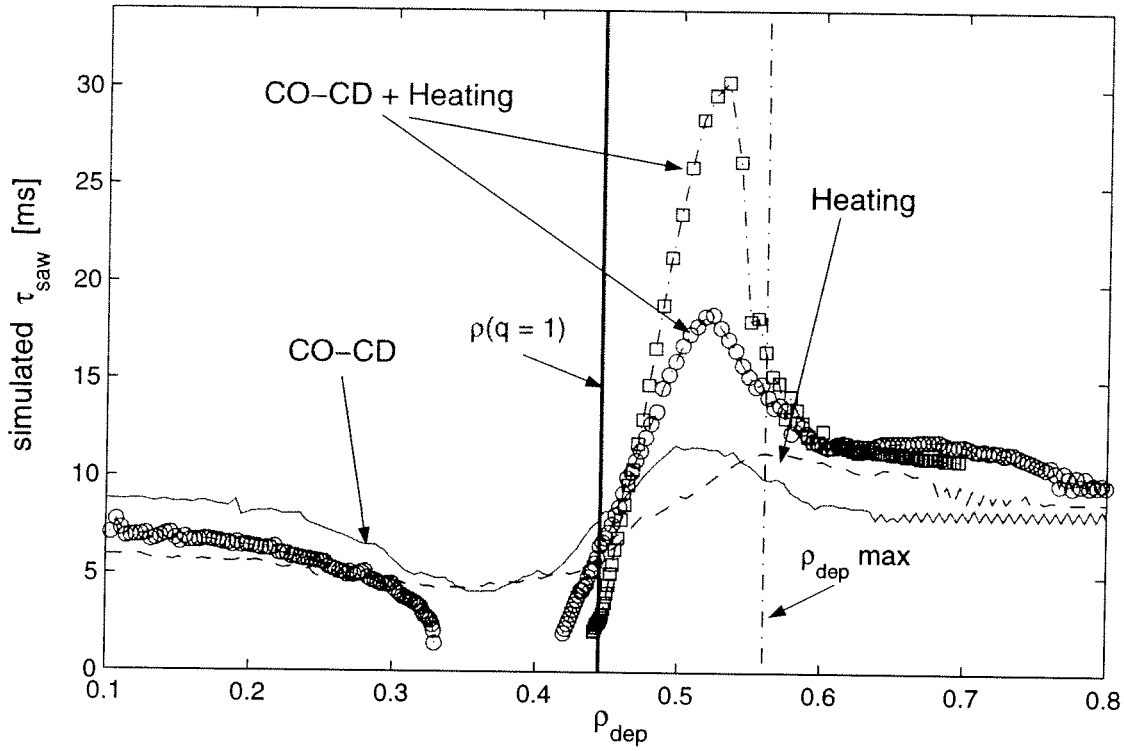

Figure 10. Simulation of the evolution of the sawtooth period versus the deposition location of a swept beam, while stabilising sawteeth with 1.35 MW ECH at ρ_{max}. The dashed line shows the sawtooth period evolution in case the swept beam produces 0.45 MW of heating, the solid line shows the case when the swept beam produces 3.5 kA of co–CD only (no heating). The dash–dotted line with open circles shows the evolution of the sawtooth period in case the swept beam produces 0.45 MW of heating *and* drives 3.5 kA of co–CD. The dash–dotted line with open squares shows the evolution of the sawtooth period when the swept beam produces 0.45 MW of heating *and* drives 10 kA of co–CD.

ramp is directly affected by CD, and this modifies the time trace of the pressure gradient at $q = 1$, although the heating power density and thereby the time evolution of the pressure profile does not change.

7. Conclusions

The effects of localised heating on the sawtooth period have been explored with a set of recent ECH discharges on the TCV device. These last experiments provide new important information on the possibilities of stabilising and destabilising sawteeth with localised heating with respect to previous results obtained on the same tokamak [18, 20].

These new experimental results have motivated a set of related simulations with a sawtooth period model included in the transport code PRETOR, which was already found in previous works [24, 25] to be consistent with the experimental behaviour observed in TCV. These simulations were aimed at identifying the separate effects of localised heating and current drive in stabilising and destabilising sawteeth.

We acknowledge that our modelling has several limitations in attempting to fully describe reality. It completely neglects two dimensional phenomena. These could play a non–negligible role, in particular when heating inside or close to the $q = 1$ surface and thereby when heating absorption occurs in plasma regions where magnetic islands are present [47]. Note that such phenomena have been found to be responsible of the different

non–triangular sawtooth period shapes observed in TCV [21]. Moreover, the inclusion of contributions coming from the density profile evolution during the sawtooth ramp could also affect, although in most cases only marginally, the values of the sawtooth periods obtained in the simulations.

Nevertheless, the general good agreement found when comparing the model predictions with all the experimental observations obtained on TCV in both ECH and ECCD experiments [23–25] allow us to state that the main physics determining the sawtooth period is captured by the model.

The results obtained in the simulations presented in this paper, as well as results obtained in previous works [23–25, 38, 45, 46] showing the agreement between the model predictions and several experimental observations collected in TCV and JET, allow us to draw general conclusions on the effects of localised heating and current drive on the sawtooth period. These can be regarded as useful guidelines for sawtooth control during tokamak operation and are generic to any auxiliary electron heating and current drive systems.

The most efficient locations which allow sawtooth stabilisation and destabilisation by means of localised heating have been identified. These are outside and inside the $q = 1$ surface respectively. In particular, PRETOR–ST simulations have shown that the heating location which maximises the sawtooth period in radial sweeps of the power deposition is closer to the $q = 1$ radius in the case of narrow deposition width as compared with the case of broader deposition. In addition it has been shown that the evolution of the sawtooth period as a function of the deposition location can indeed be used as a measurement of the deposition width as first alluded to in [18].

Consistently with previous experimental observations, the model shows that co– and counter–CD have opposite effects at symmetrical radial locations as compared with the position of the $q = 1$ surface. Inside $q = 1$ counter–CD is stabilising, whereas co–CD is destabilising. Outside $q = 1$ counter–CD is destabilising, whereas co–CD is stabilising. The addition of localised heating, which affects the sawtooth period in a similar way as the co–CD case, breaks this anti–symmetry between co– and counter–CD. Therefore the most efficient stabilisation is obtained by heating and co-CD outside $q = 1$. The most efficient destabilisation is obtained by heating and co-CD inside $q = 1$.

Furthermore, the simulations provide theoretical insights. They allow the identification of the plasma parameter involved in the model which plays the main role in determining the sawtooth period in the relevant non–ideal regime of the internal kink and which is most directly affected by localised heating and CD. This is the magnetic shear at the $q = 1$ surface, and in particular the modification of its dynamics, that is the speed at which it grows during the sawtooth ramp before reaching the critical shear, and thereby before triggering the next sawtooth crash. This is why the results presented here are not linked to EC heating and current drive but are generic to any means of localised electron heating and/or current drive near the q=1 surface.

Acknowledgements

The authors would like to acknowledge the valuable support of the whole TCV Team in performing the experiments. This work was supported in part by the Swiss National Science Foundation.

References

[1] Sauter, O., et al., Phys. Rev. Lett. **88** (2002) 105001.
[2] Sillen, R.M.J., et al., Nucl. Fusion **26** (1986) 303.

[3] Bobrovskii, G.A., Espichuk, Yu.V. and Savrukhin P.V., Fiz. Plasmy **13** (1987) 1155 [English translation Sov. J. Plasma Phys. **13** (1987) 665].
[4] TFR Group and the FOM ECRH Team, Achard, M.H., et al., Nucl. Fusion **28** (1988) 1995.
[5] Snider, R.T., et al., Phys. Fluids B **1** (1989) 404.
[6] Hanada K., et al., Phys. Rev. Lett. **66** (1991) 1974.
[7] Hanada K., et al., Phys. Fluids B **4** (1992) 3675.
[8] Alikaev, V.V., et al., in Plasma Physics and Controlled Nuclear Fusion Research 1994 (Proc. 15th Int. Conf. Seville, 1994) Vol. **1**, IAEA, Vienna (1995) 157.
[9] Ramponi, G., et al., Proc. of 13th Topical Conference on Radio Frequency Power in Plasmas, Annapolis 1999, AIP Conference Proc. **485**, ed S. Bernabei and F. Paoletti, (1999) 265.
[10] Isayama, A., Ikeda, Y., Ide, S., Suzuki, T., et al., Proc. of 14th Topical Conference on Radio Frequency Power in Plasmas, Oxnard 2001, AIP Conference Proc. **595**, ed Tak Kuen Mau and J. deGrassie, (2001) 267.
[11] Asakawa, M., Tanaka, H., et al., Fusion Eng. Des. **53** (2001) 237.
[12] Westerhof, E., Polman, R.W., et al., Fusion Eng. Des. **53** (2001) 259.
[13] Capes, H., et al., Proc. of 4th Int. Symposium on Heating in Toroidal Plasmas, (Varenna, 1984), ed H. Knoepfel, E. Sindoni, Vol. **2** (1984) 921.
[14] Zakharov, L., Rogers, B., and Migliuolo, S., Phys. Fluids B **5** (1993) 2498.
[15] Porcelli, F., Boucher, D., and Rosenbluth, M.N., Plasma Phys. Control. Fusion **38** (1996) 2163.
[16] Hofmann, F., et al., Plasma Phys. Control. Fusion **36** (1994) B277.
[17] Pietrzyk, Z.A., et al., Nucl. Fusion **39** (1999) 587.
[18] Goodman, T.P., Henderson, M.A., et al., Proc. of 26th EPS Conf. on Contr. Fusion and Plasma Physics, Maastricht, 1999, ECA Vol. **23J** (1999) 1101.
[19] Reimerdes, H., Pochelon, A., Sauter, O., et al., Plasma Phys. Control. Fusion **42** (2000) 629.
[20] Henderson, M.A., Goodman, T.P., et al., Fusion Eng. Des. **53** (2001) 241.
[21] Furno, I., Angioni, C., Porcelli, F., Weisen, H., et al., Nucl. Fusion **41** (2001) 403.
[22] Aymar, R., Plasma Phys. Control. Fusion **42** (2001) B385.
[23] Sauter, O., et al., Theory of Fusion Plasmas (Proc. Joint Varenna–Lausanne Int. Workshop) (Varenna, 1998) ed J.W. Connor, E. Sindoni and J. Vaclavik, ISPP–18 (Bologna, Editrice Compositori) (1999) 403.
[24] Angioni, C., et al., Theory of Fusion Plasmas (Proc. Joint Varenna–Lausanne Int. Workshop) (Varenna, 2000) ed J.W. Connor, O. Sauter and E. Sindoni, ISPP–19 (Bologna, Editrice Compositori) (2001) 73.
[25] Sauter, O., et al., Phys. Plasmas **8** (2001) 2199.
[26] Porcelli, F., et al., Nucl. Fusion **41** (2001) 1207.
[27] Kadomtsev, B.B., Fiz. Plasmy **1** (1975) 710 [English translation: Sov. Journal Plasma Phys. **1** (1976) 389].
[28] Boucher, D., Rebut, P.H., Proc. IAEA Tech. Com. on Advances in Simulation and Modell. of Thermonuclear Plasmas (Montreal, 1992) 142.
[29] Sauter, O., Angioni, C. and Lin–Liu, Y.R., Phys. Plasmas **6** (1999) 2834; Errata, Phys. Plasmas **9** (2002) 5140.
[30] Rebut, P.H., Lallia, P.P., and Watkins, M.L., Proc. 12th Int. Conf. on Plasma Physics and Controlled Nuclear Fusion Research, Nice 1988, IAEA Vienna 1989, Vol. **2**, p. 191.
[31] Angioni, C., *Modelling of electron transport and of sawtooth activity in tokamaks*, Ph. D. Thesis nr 2469, Ecole Polytechinique Fédérale de Lausanne (2001), 1015 Lausanne, Switzerland.
[32] Pegoraro, F., Porcelli, F., and Schep, T.J., Phys. Fluids B **1** (1989) 364.
[33] Porcelli, F., et al., Report JET-IR(88)16, JET Laboratory (1988).
[34] Cohen, R.H., Phys. Fluids **30** (1987) 2442.
[35] Matsuda. K., IEEE Trans. Plasma Sci. **PS-17**, (1989) 6.
[36] Lin-Liu, Y.R., et al., in Controlled Fusion and Plasma Physics (Proc. 26th Eur. Conf Maastricht, 1999), ECA Vol. **23J**, European Physical Society, Geneva (1999), p. 1245.
[37] Mlynar, J., et al., Plasma Phys. Control. Fusion **45** (2003) 169.
[38] Angioni, C., et al., Plasma Phys. Control. Fusion **44** (2002) 205.
[39] Bhatnagar, V.P., et al., Nucl. Fusion **34** (1994) 1579.
[40] Goodman, T.P., et al., in 1998 International Congress on Plasma Physics (Proc. Cong. Prague, 1998), Vol. 22C, Eurpean Physical Society, Geneva (1998) 1324.
[41] Goodman, T.P., et al., *Overview of TCV results*, submitted to Nucl. Fusion (2003).
[42] Henderson, M.A., Alberti, S., Angioni C., et al., Phys. Plasmas **10** (2003) 1796;
[43] Hofmann, F., Tonetti, G., Nucl. Fusion **28** (1988) 1871.
[44] Mück, A., et al., Proc. 29th EPS Conf. on Control. Fusion and Plasma Physics, (Montreux, 2002), ECA Vol **26**, P 1.037 (http://epsppd.epfl.ch).

[45] Mantsinen, M.J., et al., Plasma Phys. Control. Fusion **44** (2002) 1521.
[46] Angioni, C., et al., *Understanding sawtooth period behaviour with electron and ion resonance heating and current drive*, Proc. 29th EPS Conf. on Control. Fusion and Plasma Physics, (Montreux, 2002), ECA Vol **26**, P 1.118 (http://epsppd.epfl.ch).
[47] Porcelli, F., et al., Phys. Rev. Lett. **82** (1999) 1458.